Int. J. Solids Structures Vol. 24, No. 9, pp. 915–936, 1988
Printed in Great Britain.

0020–7683/88 $3.00+ .00

INTERACTION FUNCTIONS OF A RIGID STRIP BONDED TO SATURATED ELASTIC HALF-SPACE

MUMTAZ K. KASSIR and JIMIN XU
Department of Civil Engineering, City College of City University of New York, NY 10031, U.S.A.

(*Received* 11 *September* 1987; *in revised form* 2 *March* 1988)

Abstract—A comprehensive analytical solution is developed to generate the interaction functions of a rigid permeable strip in contact with a saturated porous elastic half-space. Linear hysteretic damping characteristics of the medium are included in the formulation. The mixed boundary-value problem of a welded (and smooth) surface footing is reduced to a set of coupled Fredholm integral equations of the first kind and a numerical solution is provided. Frequency-dependent interaction functions (stiffnesses and radiation damping coefficients) of a medium modelling a saturated dense sand are computed and exhibited graphically to reveal the influence of pore water, permeability effects and hysteretic damping characteristics of the medium. In the horizontal mode of response and without hysteretic damping, the pore water causes the effective stiffness to increase by 50–100% while it has negligible influence on the damping coefficient. With 5% hysteretic damping, the horizontal stiffness changes sign and character and there is an increase of about 25% in its magnitude compared to the corresponding dry case. For the vertical and rocking modes of response, the impact of pore water on the interaction functions (both stiffnesses and damping coefficients) is much more pronounced. Without hysteretic damping, there are changes in sign in the stiffnesses of the medium, and the magnitudes of the interaction functions, relative to the corresponding dry case, could be as large as several folds, especially for the higher values of the dimensionless frequency. At 5% damping, the effective stiffnesses are increased by about 25–50% while the damping coefficients almost double. Concerning the influence of types of contact, the interaction functions are practically identical for smooth and welded contacts over the frequency range of interest. The results are useful in determining the response of surface structures to seismic excitation, in particular, where the ground water is at a level to impact such response.

1. INTRODUCTION

A topic of considerable interest in understanding the interaction between soil and structure is the dynamic force–displacement relationship of a rigid footing attached to a half-space. Such relationships, when expressed as influence functions or interaction coefficients, reduce the problem of finding the dynamic response of surface structures to a set of algebraic equations derived from the Newtonian equations of motion of the structure's model. They play a key role in any seismic response analysis and in the study of machine vibrations.

For an elastic half-space, a considerable amount of work has been done on the topic beginning with the work of Lamb (1904). Several analytical techniques, such as integral transforms, Green's functions, etc., as well as finite element and other numerical methods have been developed to treat various aspects of the topic. Confining attention to the analytical work and citing a few of the recent references, Collins (1962) discussed the torsional oscillations of a rigid disk attached to a semi-infinite solid. Awjobi and Grootenhuis (1965), Zakorko and Rostovtsev (1965), Robertson (1966) and Gladwell (1968) investigated the vertical, tangential and/or rocking oscillations of a smooth disk in contact with a half-space. Karasudhi *et al.* (1968) determined the force–displacement relationships due to harmonic oscillations of a smooth rectangular footing at the surface of a half-space. The corresponding problem of a welded footing was examined by Luco and Westmann (1972) and some limited numerical results were obtained. Utilizing a formulation suggested by Thau (1967) and approximating the contact stresses, Oien (1970) obtained a solution for a welded (and smooth) rectangular oscillator undergoing basic modes of motion. The solution, which gives accurate results for a smooth footing, is also valid over the frequency range of interest in seismic response analysis.

When the medium consists of an elastic soil saturated by ground water, usually referred to as a two-phase medium, there is a conspicuous lack of analytical solutions needed to provide meaningful insight into the impact of the soil–water system on the seismic

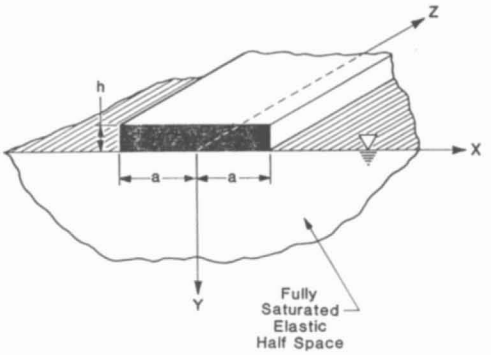

Fig. 1. Rigid strip in contact with a saturated elastic half-space.

response of surface footings. The basic equations governing the propagation of waves in such a medium were developed by Biot (1956, 1962). Biot's theory takes into account the effects of fluid viscosity and compressibility and gives rise to coupling between the solid and fluid states of stress. In this theory, three types of waves are found to exist in the infinite medium two dilatational and one shear wave. The first of the dilatational waves propagates like the compression wave in an elastic solid with little dispersion, while the second dilatational wave is highly attenuated and travels at a much slower rate. Because the trapped mass of fluid in the pores of the solid skeleton changes with time, the shear wave velocity is influenced by the permeability of the fluid and the elastic characteristics of the matrix material. The presence of Rayleigh-type surface waves in Biot's field equations were investigated by Jones (1961) and Deresiewicz (1962). To the best knowledge of the authors, there are no dynamic half-plane analytical solutions to Biot's general field equations. Paul (1976a, b) solved some transient, two-dimensional surface loading problems where the dissipation effect of the fluid, represented by the viscosity term in Biot's equations, is neglected. Such solutions are of limited practical use in determining the seismic response of a saturated soil to surface footings. Finite element methods have been applied by Lung (1980) and Costantino (1986) to solve half-plane wave propagation problems for the two-phase medium. Although damping characteristics of the medium were included in the formulation, the interaction coefficients were generated for a medium without structural damping. These authors conclude that the dissipation of the pore water significantly affects the interaction coefficients over the frequency range of interest. It should be pointed out that the oscillations in their results are due to the numerical nature of satisfying the radiation condition in finite element methods (see also Das Gupta (1980)).

The aim of this paper is to generate the interaction coefficients (both stiffnesses and radiation damping coefficients) for a two-phase elastic medium. A two-dimensional plane strain configuration is considered with a rigid permeable surface footing undergoing harmonic oscillations as shown in Fig. 1. The solid skeleton is assumed linearly elastic with hysteretic damping characteristics while the fluid is viscous and compressible. Biot's generalized field equations govern the motions in the solid and fluid parts of the medium. The plan of the paper is as follows: Section 2 contains the basic equations governing the wave propagation. Linear hysteretic damping properties of the system have been included in the constitutive equations to account for nonlinearities in the modelling of the medium as is customarily done in soil–structure interaction problems. In Section 3, the compressive and shear waves are separated, and the integral transform solution is derived. The hysteretic damping ratios for normal and shearing strains are assumed identical. Section 4 contains solutions of the displacement fields due to vibratory surface line loads. These solutions are used as Green's functions to formulate the contact problem. The formulation of the problem of a permeable rigid strip in contact with the half-plane is carried out in Section 5. Here, the procedure employed follows the one suggested by Thau (1967) and Oien (1970). Utilizing the previously determined Green's functions and approximating the contact stresses beneath the strip by square root singularity characteristics, the problem of determining the influence functions for a welded (and smooth) footing is reduced in Section 6 to coupled Fredholm

integral equations of the first kind. To facilitate the numerical work, the integral equations are then transformed into algebraic equations. Finally, Section 7 contains the numerical results of the interaction coefficients of a typical medium consisting of saturated dense sand and a discussion of the results, in particular, the modifications due to pore water and damping characteristics of the system are pointed out.

2. BASIC EQUATIONS

Consider an element of a two-phase elastic material consisting of solid particles and pore fluid. With reference to Cartesian coordinates, denote the components of the solid displacement vector by u_j and those of the fluid portion by $U_j (j = x, y, z)$. The latter components are defined such that the volume of fluid displaced through unit areas normal to reference axes are fU_j where f designates the porosity of the medium. The displacement components of the fluid relative to the solid and measured in terms of the volume per unit area of the bulk material are $w_j = f(U_j - u_j)$. Because of its occurrence in a variety of applications, the problem is viewed as one in plane strain, namely, a saturated half-space bounded by the plane $y = 0$ and occupying the region $y \geqslant 0$, $|x| < \infty$, $|z| < \infty$.

Based upon Biot's classical formulation (1962), the pore pressure (p) in the medium is given by the relation

$$p = \alpha'(-\alpha e + \varepsilon) \tag{1}$$

in which α, α' represent the compressibilities of the solid and fluid particles, respectively, and e, ε are the corresponding solid dilatation and fluid volumetric strains defined as

$$e = \partial u_x/\partial x + \partial u_y/\partial y \tag{2a}$$

$$\varepsilon = -(\partial w_x/\partial x + \partial w_y/\partial y). \tag{2b}$$

Inasmuch as the present work is motivated by determining the response of a soil–structure system to dynamic loading, the structural damping properties of the medium are included in the constitutive equations. Assuming linear hysteretic damping ratios, it follows that the components of the bulk stress tensor are related to the displacements and velocities through the relations

$$\tau_{xx} = E_c(\partial u_x/\partial x + c_1 \partial u_y/\partial y) - \alpha p + \lambda_c E_c(\partial \dot{u}_x/\partial x + c_1 \partial \dot{u}_y/\partial y) \tag{3a}$$

$$\tau_{yy} = E_c(c_1 \partial u_x/\partial x + \partial u_y/\partial y) - \alpha p + \lambda_c E_c(c_1 \partial \dot{u}_x/\partial x + \partial \dot{u}_y/\partial y) \tag{3b}$$

$$\tau_{xy} = c_2 E_c[\partial u_x/\partial y + \partial u_y/\partial x + \lambda_s(\partial \dot{u}_x/\partial y + \partial \dot{u}_y/\partial x)] \tag{3c}$$

where the terms containing λ_c and λ_s represent, respectively, the hysteretic damping ratios associated with the normal and shearing strains; c_1, c_2 and E_c (confined modulus) are constants depicting the elastic characteristics of the material and are defined as follows:

$$c_1 = \nu/(1-\nu) \tag{4a}$$

$$2c_2 = 1 - c_1 \tag{4b}$$

$$E_c = (1-\nu)E/(1+\nu)(1-2\nu) \tag{4c}$$

$$E_c c_2 = \mu. \tag{4d}$$

Here, E, μ and ν designate the modulus of elasticity, shearing modulus and Poisson's ratio of the solid skeleton, respectively. In eqns (3), a dot over a symbol indicates differentiation with respect to the time variable (t).

The governing equations of small motion at a point in the two-phase medium are

$$\frac{\partial \tau_{xx}}{\partial x}+\frac{\partial \tau_{xy}}{\partial y}=\rho \ddot{u}_x+\rho' \ddot{w}_x \tag{5a}$$

$$\frac{\partial \tau_{xy}}{\partial x}+\frac{\partial \tau_{yy}}{\partial y}=\rho \ddot{u}_y+\rho' \ddot{w}_y \tag{5b}$$

for the bulk stresses, and

$$-\frac{\partial p}{\partial x}=\rho' \ddot{u}_x+\frac{1}{f}\rho' \ddot{w}_x+\frac{\gamma'}{k}\dot{w}_x \tag{6a}$$

$$-\frac{\partial p}{\partial y}=\rho' \ddot{u}_y+\frac{1}{f}\rho' \ddot{w}_y+\frac{\gamma'}{k}\dot{w}_y \tag{6b}$$

for the pore pressure. In eqns (5) and (6), ρ designates the mass density of the composite solid–fluid medium, ρ' the mass density of the fluid and γ', k are, respectively, the unit weight of the fluid and the coefficient of permeability. In Biot's work, the term γ'/k is replaced by η/k where η and k are Biot's definition of the fluid viscosity and permeability, respectively. The notation adopted here is more commonly used in the current terminology of soil mechanics. Upon neglecting the inertia terms in eqns (6) there result Darcy's well-known laws governing the seepage of fluid in soils. It should also be mentioned that the aforementioned formulation is valid for low frequency motions where the assumptions of laminar or Poiseuille flow hold. For a typical sandy medium, the cutoff frequency is about 100 Hz, well beyond any frequency range of practical interest in soil–structure interaction problems. Further details can be found in Biot's original work (1962).

Inserting relations (1)–(4) into eqns (5) and (6) renders

$$V_c^2\frac{\partial}{\partial x}(e-\alpha k\varepsilon)+V_s^2\frac{\partial \Omega}{\partial y}=\ddot{u}_x+N\ddot{w}_x-\frac{E_c}{\rho}\left[\lambda_c\frac{\partial^2 \dot{u}_x}{\partial x^2}+c_2\lambda_s\frac{\partial^2 \dot{u}_x}{\partial y^2}+(c_1\lambda_c+c_2\lambda_s)\frac{\partial^2 \dot{u}_y}{\partial x\,\partial y}\right] \tag{7a}$$

$$V_c^2\frac{\partial}{\partial y}(e-\alpha k\varepsilon)-V_s^2\frac{\partial \Omega}{\partial x}=\ddot{u}_y+N\ddot{w}_y-\frac{E_c}{\rho}\left[c_2\lambda_s\frac{\partial^2 \dot{u}_y}{\partial x^2}+\lambda_c\frac{\partial^2 \dot{u}_y}{\partial y^2}+(c_1\lambda_c+c_2\lambda_s)\frac{\partial^2 \dot{u}_x}{\partial x\,\partial y}\right] \tag{7b}$$

$$KV_c^2\frac{\partial}{\partial x}(\alpha e-\varepsilon)=N\ddot{u}_x+\frac{N}{f}\ddot{w}_x+\frac{\gamma'}{k\rho}\dot{w}_x \tag{7c}$$

$$KV_c^2\frac{\partial}{\partial y}(\alpha e-\varepsilon)=N\ddot{u}_y+\frac{N}{f}\ddot{w}_y+\frac{\gamma'}{k\rho}\dot{w}_y \tag{7d}$$

in which, $\Omega=\partial u_x/\partial y-\partial u_y/\partial x$, designates the rotation of an element of the solid skeleton, $N=\rho'/\rho$, V_c and V_s are compressional and shear velocities of the bulk material, respectively, and K is a dimensionless modulus. They are defined as follows

$$V_c^2=(E_c+\alpha^2\alpha')/\rho \tag{8a}$$

$$V_s^2=\mu/\rho \tag{8b}$$

$$K=\alpha'/(E_c+\alpha^2\alpha'). \tag{8c}$$

Equations (7) represent the displacement equations of motion governing the propagation of elastic waves in a saturated porous material possessing linear hysteretic damping. In an unbounded domain, these equations give rise to two distinct dilatational waves and one distortional wave which are coupled through the hysteretic damping. In order to decompose the waves into dilatational and distortional ones, it is necessary to assume that the normal hysteretic damping ratio is identical to the shearing strain one, i.e. $\lambda_s=\lambda_c$. Although these

two damping ratios are most probably not equal in an actual material, they do not vary significantly from each other in typical soil materials, and the previous assumption is usually made in analyzing soil–structure iteration problems.

3. COMPRESSIVE AND SHEAR WAVES

In order to determine the equations of propagation governing the compressive and shear waves, the following substitutions are introduced into eqns (7):

$$u_x = \partial\phi_s/\partial x + \partial\psi_s/\partial y \tag{9a}$$

$$u_y = \partial\phi_s/\partial y - \partial\psi_s/\partial x \tag{9b}$$

$$w_x = \partial\phi_f/\partial x + \partial\psi_f/\partial y \tag{9c}$$

$$w_y = \partial\phi_f/\partial y - \partial\psi_f/\partial x. \tag{9d}$$

It is found that the compressive waves are governed by

$$V_c^2\nabla^2\left(\phi_s + \alpha k\phi_f + \frac{k}{\alpha'}E_c\lambda_c\dot{\phi}_s\right) = \ddot{\phi}_s + N\ddot{\phi}_f \tag{10a}$$

$$KV_c^2\nabla^2(\alpha\phi_s + \phi_f) = N\ddot{\phi}_s + \frac{N}{f}\ddot{\phi}_f + \frac{\gamma'}{k\rho}\dot{\phi}_f \tag{10b}$$

while the shear wave is obtained from the set

$$V_s^2\nabla^2(\psi_s + \lambda_c\dot{\psi}_s) = \ddot{\psi}_s + N\ddot{\psi}_s \tag{11a}$$

$$-\left(\frac{\gamma'}{k\rho}\right)\dot{\psi}_f = N\ddot{\psi}_s + \frac{N}{f}\ddot{\psi}_f. \tag{11b}$$

For vibratory loading introduced at the boundary of the half-space with harmonic time dependence $e^{i\omega t}$, ω being the applied frequency, eqns (10) and (11) admit exponential solutions, appropriate to propagation of waves in the medium, of the form

$$(\phi_s, \phi_f, \psi_s, \psi_f) \sim e^{-ny + i(sx+\omega t)} \tag{12}$$

where n is as yet an unknown complex parameter and s and ω are real. In order to insure bounded displacements and stresses at remote distance and outward waves propagating from the source (radiation condition), the following requirements must be satisfied:

$$\text{Re } n \geqslant 0 \quad \text{and} \quad \text{Im } n \geqslant 0. \tag{13}$$

Substituting expression (12) into eqns (10) and carrying out the necessary algebraic work, it is found that (omitting the term $e^{i\omega t}$ for brevity)

$$\begin{Bmatrix}\phi_s\\ \phi_f\end{Bmatrix} = e^{isx}\sum_{j=1}^{2}\begin{Bmatrix}1\\ a_j\end{Bmatrix}\phi_j(s)\, e^{-n_j y} \tag{14}$$

where $\phi_j(s), j = 1, 2$, are arbitrary transform coefficients and the exponents, n_j, are defined as

$$\left.\begin{aligned} n_j &= \sqrt{(s^2-\omega^2/V_j^2)} \\ \operatorname{Re} n_j &\geqslant 0, \quad j=1,2 \\ \operatorname{Im} n_j &\geqslant 0, \quad j=1,2. \end{aligned}\right\} \tag{15}$$

The "velocities", V_j, and the coefficients, a_j, $j = 1, 2$ in eqns (14) and (15) are complex-valued functions of the material parameters and the applied frequency, and are given in Appendix A. In a similar manner, the shear wave is found to be governed by the potential functions

$$\begin{Bmatrix} \psi_s \\ \psi_f \end{Bmatrix} = \phi_3(s)\, e^{-n_3 y + isx} \begin{Bmatrix} 1 \\ a_3 \end{Bmatrix}. \tag{16}$$

Here, the exponent, n_3, stands for

$$\left.\begin{aligned} n_3 &= \sqrt{(s^2-\omega^2/V_3^2)} \\ \operatorname{Re} n_3 &\geqslant 0 \quad \text{and} \quad \operatorname{Im} n_3 \geqslant 0 \end{aligned}\right\} \tag{17}$$

and quantities V_3 and a_3 are abbreviated in Appendix A.

Utilizing eqns (9) in conjunction with expressions (14) and (16), it is readily shown that the expressions for the displacements are

$$u_x = (is\phi_1\, e^{-n_1 y} + is\phi_2\, e^{-n_2 y} + n_3\phi_3\, e^{-n_3 y})\, e^{isx} \tag{18a}$$

$$u_y = (-n_1\phi_1\, e^{-n_1 y} - n_2\phi_2\, e^{-n_2 y} + is\phi_3\, e^{-n_3 y})\, e^{isx} \tag{18b}$$

$$w_x = (ia_1 s\phi_1\, e^{-n_1 y} + ia_2 s\phi_2\, e^{-n_2 y} + a_3 n_3\phi_3\, e^{-n_3 y})\, e^{isx} \tag{18c}$$

$$w_y = (-n_1 a_1\phi_1\, e^{-n_1 y} - n_2 a_2\phi_2\, e^{-n_2 y} + isa_3\phi_3\, e^{-n_3 y})\, e^{isx} \tag{18d}$$

and those for the pore pressure and bulk stresses immediately follow from eqns (1)–(3). They are

$$p = \alpha'\omega^2\, e^{isx} \sum_{j=1}^{2} \left(\frac{\alpha + a_j}{V_j^2}\right)\phi_j(s)\, e^{-n_j y} \tag{19a}$$

$$\tau_{xy} = -\mu(1+i\omega\lambda_c)[2is(n_1\phi_1\, e^{-n_1 y} + n_2\phi_2\, e^{-n_2 y}) - (s^2+n_3^2)\phi_3\, e^{-n_3 y}]\, e^{isx} \tag{19b}$$

$$\tau_{yy} = -\mu(1+i\omega\lambda_c)\left[\sum_{j=1}^{2}\left\{2s - \left\langle c_2 + \frac{\alpha\alpha'(\alpha+a_j)}{\mu(1+i\omega\lambda_c)}\right\rangle \frac{\omega^2}{V_j^2}\right\}\phi_j\, e^{-n_j y} - 2n_3\phi_3\, e^{-n_3 y}\right] e^{isx}. \tag{19c}$$

The unknown coefficients ϕ_j, $j = 1, 2, 3$ are determined from the particular boundary conditions of the problem. Also in eqns (18) and (19), as in the sequel, the term $e^{i\omega t}$ is omitted.

4. VIBRATORY SURFACE LOADS

When the surface of the half-space is subjected to a distribution of normal periodic loading described by the relations

$$p(x,0) = \tau_{xy}(x,0) = 0 \tag{20a}$$

$$\tau_{yy}(x,0) = \tau_0\, e^{isx}, \quad \tau_0 = \text{constant} \tag{20b}$$

then it can be concluded from eqns (19) that

$$\phi_1 = \beta_2(s^2+n_3^2)\tau_0/\mu F(s) \tag{21a}$$

$$\phi_2 = -\beta_1\phi_1/\beta_2 \tag{21b}$$

$$\phi_3 = 2is(\beta_1 n_2-\beta_2 n_1)\tau_0/\mu F(s) \tag{21c}$$

in which $F(s)$ designates the Rayleigh function

$$F(s) = 2(1+i\omega\lambda_c)[(s^2+n_3^2)(s^2-\gamma\omega^2/V_c^2)+2n_3 s^2(\beta_1 n_2-\beta_2 n_1)] \tag{22}$$

and β_j, $j = 1,2$ and γ are frequency-dependent abbreviations introduced for algebraic convenience and are available in Appendix A. The expressions of the displacement components can easily be computed from eqns (18) and (21).

The response to a concentrated line load of magnitude P per unit length of strip, acting parallel to the y-axis at $x = z = 0$, is obtained by setting $\tau_0 = -(P/2\pi)\,ds$ in eqns (21) and integrating the resulting expressions over the interval $(-\infty, \infty)$. It follows that the surface values of the displacements are given by

$$u_x(x,0) = -\frac{iP}{2\pi\mu}\int_{-\infty}^{\infty}\frac{sF_1(s,\omega)}{F(s,\omega)}\,e^{isx}\,ds \tag{23a}$$

$$u_y(x,0) = -\frac{P}{2\pi\mu}\int_{-\infty}^{\infty}\frac{(\beta_2 n_1-\beta_1 n_2)\omega^2/V_3^2}{F(s,\omega)}\,e^{isx}\,ds \tag{23b}$$

where

$$F_1(s,\omega) = s^2+n_3^2+2n_3(\beta_1 n_2-\beta_2 n_1). \tag{24}$$

In a similar manner, the expressions of the surface displacements due to a concentrated tangential load of magnitude (H) per unit length, acting at the origin parallel to the x-axis, are

$$u_x(x,0) = \frac{H}{\pi\mu}\int_{-\infty}^{\infty}\frac{\gamma n_3\omega^2/V_c^2}{F(s,\omega)}\,e^{isx}\,ds \tag{25a}$$

$$u_y(x,0) = \frac{iH}{2\pi\mu}\int_{-\infty}^{\infty}\frac{sF_2(s,\omega)}{F(s,\omega)}\,e^{isx}\,ds. \tag{25b}$$

Here

$$F_2(s,\omega) = \omega^2/V_3^2-\gamma\omega^2/V_c^2+F_1(s,\omega) \tag{26}$$

and γ is available in Appendix A. In the sequel, integral expressions (23) and (25) are used as Green's functions for the displacement components in the half-space in order to generate the influence functions. In these integrals, the requirements $\mathrm{Re}\,n_j \geqslant 0$ and $\mathrm{Im}\,n_j \geqslant 0$, $j = 1,2,3$, must always be maintained to insure the requirements of the radiation condition. In the complex s-plane, a proper interpretation of the integrals in the expressions of Green's functions would require branch cuts to be taken along the arcs $\mathrm{Re}\,n_j = 0$ through the complex branch points ω/V_j, $j = 1,2,3$. Also, the complex poles of the Rayleigh function, $F(s,\omega)$, must be determined and contour integration performed. However, in this case, the function $F(s,\omega)$ has no real roots and the integrals are well defined as the integrals are finite throughout the range of validity of the integrals, namely, the real s-axis.

5. A RIGID STRIP IN CONTACT WITH A HALF-SPACE

This section contains an outline of the formulation employed to determine the influence functions which characterize the dynamic interaction of a mobile structure in contact with a saturated half-space. Once the influence functions are known, the response to harmonic excitation in the half-space is simply reduced to solving a set of algebraic equations obtained from the Newtonian equations of motion of the structure's model.

Consider a rigid strip of half-width a in contact with the half-space and subjected to the modes of motions shown in Fig. 1. The formulation suggested by Thau (1967) and Oien (1970) is adopted here. Similar techniques have previously been used by Junger (1953) and Smith (1962) in analyzing the effect of acoustic waves on structures immersed in fluids. The desired solution is sought in two steps: the first step involves the radiation of waves into the soil half-space by the strip vibrating as a rigid body, and the second determines the diffraction of the incident waves by a fixed strip. Since the influence functions needed to determine the dynamic interaction between structure and the surrounding medium are obtained from the radiation solution, attention is focused on this part of the formulation. Additional details are available in the cited references.

For an incident displacement in the solid skeleton, $\mathbf{u}^{\mathrm{I}}(x, y)$, it is required to construct a scattered field, $\mathbf{u}^{\mathrm{S}}(x, y)$, such that beneath the strip the following condition holds:

$$\mathbf{u}^{\mathrm{I}}(x,0)+\mathbf{u}^{\mathrm{S}}(x,0) = U\mathbf{e}_x+(V+x\theta)\mathbf{e}_y. \tag{27}$$

The right-hand side of eqn (27) defines the rigid body motion of the base of the strip, i.e. U, V and θ are, respectively, the horizontal displacement, vertical displacement and angular rotation about the mass center of the strip, and $\mathbf{e}_x$ and $\mathbf{e}_y$ are the unit base vectors. The factor $\mathrm{e}^{\mathrm{i}\omega t}$ in eqn (27) is, of course, implied but omitted for brevity. In the region $|x| > a$ of the boundary, the surface tractions associated with the scattered field are required to vanish. This describes the boundary conditions for perfect contact between the strip and half-space. For partial or smooth contact, additional stresses must vanish beneath the strip, namely shearing stress for vertical and rocking motions and normal stress for horizontal motion. Upon specifying the incident field, eqn (27) becomes

$$\mathbf{u}^{\mathrm{S}}(x,0) = (U-Q_x\,\mathrm{e}^{-\omega x/d})\mathbf{e}_x+(V+x\theta-Q_y\,\mathrm{e}^{-\omega x/d})\mathbf{e}_y \tag{28}$$

where Q_x and Q_y are complex-valued functions specifying the amplitude and phase of the incident motion, and d is the apparent velocity of the incident wave observed on the free surface.

As mentioned previously the scattered field is determined in two parts, $\mathbf{u}_1^{\mathrm{S}}(x, y)$ and $\mathbf{u}_2^{\mathrm{S}}(x, y)$, and each part can be decomposed into symmetric and antisymmetric components about the $x = 0$ plane. Thus, in the region $y = 0$, $|x| \leqslant a$

$$\mathbf{u}_1^{\mathrm{S}}(x,0) = Q_x[\mathbf{u}^{(1)}+\mathbf{u}^{(2)}]+Q_y[\mathbf{u}^{(3)}+\mathbf{u}^{(4)}] \tag{29a}$$

$$\mathbf{u}_2^{\mathrm{S}}(x,0) = U\mathbf{u}^{(5)}+V\mathbf{u}^{(6)}+x\theta\mathbf{u}^{(7)}. \tag{29b}$$

Associated with the scattered displacements $\mathbf{u}^{(j)}$ in eqns (29), there are surface tractions $\tau_{yy}^{(j)}(x,0) = \sigma^{(j)}(x)$ and $\tau_{xy}^{(j)}(x,0) = \tau^{(j)}(x)$ beneath the strip to be determined. Consideration of equilibrium of the weightless rigid strip requires that

$$F^{(j)} = \int_{-a}^{a} \sigma^{(j)}(x)\,\mathrm{d}x \tag{30a}$$

$$H^{(j)} = \int_{-a}^{a} \tau^{(j)}(x)\,\mathrm{d}x \tag{30b}$$

$$M^{(j)} = \int_{-a}^{a} x\sigma^{(j)}(x)\,\mathrm{d}x. \tag{30c}$$

Here, $F^{(j)}$, $H^{(j)}$ and $M^{(j)}$ represent, respectively, the amplitude per unit length of the vertical force, horizontal force and moment acting on the strip. By virtue of the existing symmetry implied in the problem, it is readily concluded from eqns (30) that $F^{(j)} = 0$ for $j = 1, 3, 5, 7$ while for $j =$ even, $H^{(j)} = M^{(j)} = 0$. The remaining eleven forces and moments, namely, $F^{(j)}$ for $j = 2, 4, 6$ and $H^{(j)}$ and $M^{(j)}$ for $j = 1, 3, 5, 7$ constitute the complete set of influence functions. These functions give rise to the following forces and moments:

$$F^s = Q_x F^{(2)} + Q_Y F^{(4)} + V F^{(6)} \tag{31a}$$

$$H^s = Q_x H^{(1)} + Q_Y H^{(3)} + U H^{(5)} + \theta H^{(7)} \tag{31b}$$

$$M^s = Q_x M^{(1)} + Q_Y M^{(3)} + U M^{(5)} + 8 M^{(7)}. \tag{31c}$$

In eqns (31), the influence functions obtained from the immobile strip (terms with $j = 1, 2, 3, 4$) provide the loads which force the motion of the mobile strip. The remaining terms ($j = 5, 6, 7$) represent the resistance of the half-space to the motion of the strip, and these are the desired interaction coefficients in soil–structure interaction problems. Numerical values of these functions are determined in the sequel, and can be used as the foundation's interaction spring-dashpot coefficients in carrying out the analysis of a structure and its surroundings.

6. INFLUENCE FUNCTIONS

By use of Green's functions for the saturated half-space, the problem of determining the unknown surface tractions, $\sigma^{(j)}(x)$ and $\tau^{(j)}(x)$, is reduced to the solution of two coupled integral equations valid for $|x| \leqslant a$, namely

$$\int_{-a}^{a} \tau^{(j)}(\xi) u_x^H(x-\xi)\, \mathrm{d}\xi + \int_{-a}^{a} \sigma^{(j)}(\xi) u_x^P(x-\xi)\, \mathrm{d}\xi = u_x^{(j)}(x) \tag{32a}$$

$$\int_{-a}^{a} \tau^{(j)}(\xi) u_y^H(x-\xi)\, \mathrm{d}\xi + \int_{-a}^{a} \sigma^{(j)}(\xi) u_y^P(x-\xi)\, \mathrm{d}\xi = u_y^{(j)}(x). \tag{32b}$$

In eqns (32), Green's functions u_x^P and u_y^P, are obtained from eqns (23) by setting $P = 1$ and similarly u_x^H and u_y^H are available from expressions (25). As a preliminary to the numerical evaluation, eqns (32) are placed in non-dimensional form by scaling the independent variables against the length (a), i.e.

$$x = a\bar{x}, \quad \xi = a\bar{\xi}, \quad \bar{s} = as, \quad \bar{\sigma}^{(j)}(\bar{\xi}) = \sigma^{(j)}(a\bar{\xi}), \text{ etc.} \tag{33}$$

It follows that

$$\int_{-1}^{1} \bar{\tau}^{(j)}(\bar{\xi}) u_x^H(\bar{x}-\bar{\xi})\, \mathrm{d}\bar{\xi} + \int_{-1}^{1} \bar{\sigma}^{(j)}(\bar{\xi}) u_x^P(\bar{x}-\bar{\xi})\, \mathrm{d}\bar{\xi} = \frac{1}{a} u_x^{(j)}(a\bar{x}) \tag{34a}$$

$$\int_{-1}^{1} \bar{\tau}^{(j)}(\bar{\xi}) u_y^H(\bar{x}-\bar{\xi})\, \mathrm{d}\bar{\xi} + \int_{-1}^{1} \bar{\sigma}^{(j)}(\bar{\xi}) u_y^P(\bar{x}-\bar{\xi})\, \mathrm{d}\bar{\xi} = \frac{1}{a} u_y^{(j)}(a\bar{x}). \tag{34b}$$

Equations (34) constitute a pair of coupled inhomogeneous Fredholm integral equations of the first kind for the unknown contact stresses in the region $|\bar{x}| \leqslant 1$. A numerical solution to these equations can be achieved by postulating a proper series expansion for the contact stresses, which would reflect the essential characteristics of the solution, and would yield a set of independent algebraic equations for the unknown coefficients in the expansion.

From the mathematical viewpoint, it is reasonable to expect the contact stresses, in case of welded footing, to possess an oscillatory singularity of the type $r^{-1/2} \sin(\varepsilon_0 \ln r)$ where r is the small distance from the edge of the footing and ε_0 is a constant which depends

on Poisson's ratio of the solid material of the medium. This follows from the classical work of Muskhelishvili (1953) and Williams (1959) and also the work of Luco and Westmann (1972) for the dry half-space. For a smooth contact beneath the strip, the oscillatory part of the singularity disappears and only the square root part ($r^{-1/2}$) remains. Practically speaking, most of the relevant information needed for interaction analysis can be obtained by assuming a dominant square root singularity in the contact stresses for all types of contacts. In view of these observations, the following representation of the unknown contact stresses are assumed ($|\bar{x}| \leqslant 1$):

$$\bar{\tau}^{(j)}(\bar{x}) = \sum_{n=0}^{\infty} A_n^{(j)}(1-\bar{x}^2)^{-1/2}T_n(\bar{x}) \tag{35a}$$

$$\bar{\sigma}^{(j)}(\bar{x}) = \sum_{n=0}^{\infty} B_n^{(j)}(1-\bar{x}^2)^{-1/2}T_n(\bar{x}) \tag{35b}$$

where $T_n(\bar{x})$ are the Chebyshev polynomials. With this representation, a square root singularity in the contact stresses is implied, and a standard numerical scheme can be adopted to reduce eqns (34) into algebraic equations for the unknown coefficients A_n and B_n.

Inserting series expansions (35) into eqns (34), making use of the Green's functions and utilizing the well-known relations (Erdelyi *et al.*, 1954):

$$\int_{-1}^{1}(1-\bar{x}^2)^{-1/2}T_n(\bar{x})\,e^{\mp i\bar{s}\bar{x}}\,d\bar{x} = (-i)^n\pi J_n(\pm\bar{s}) \tag{36}$$

where J_n are the usual Bessel functions of the first kind of order n, it follows that

$$\sum_{n=0}^{\infty} A_n^{(j)}\frac{j^n}{2}\int_{-\infty}^{\infty}\frac{2\gamma\omega_c^2\bar{n}_3(\bar{s})}{F(\bar{s})}J_n(\bar{s})\,e^{i\bar{s}\bar{x}}\,d\bar{s} - \sum_{m=0}^{\infty} B_m^{(j)}\frac{i^{m+1}}{2}\int_{-\infty}^{\infty}\frac{\bar{s}F_1(\bar{s})}{F(\bar{s})}J_m(\bar{s})\,e^{i\bar{s}\bar{x}}\,d\bar{s} = \frac{\mu}{a}u_x^{(j)}(a\bar{x}) \tag{37a}$$

$$\sum_{m=0}^{\infty} A_n^{(j)}\frac{i^{n+1}}{2}\int_{-\infty}^{\infty}\frac{\bar{s}F_2(\bar{s})}{F(\bar{s})}J_n(\bar{s})\,e^{i\bar{s}\bar{x}}\,d\bar{s} + \sum_{m=0}^{\infty} B_m^{(j)}\frac{i^m}{2}\int_{-\infty}^{\infty}\frac{[\beta_2\bar{n}_1(\bar{s})-\beta_1\bar{n}_2(\bar{s})]\omega_3^2}{F(\bar{s})}J_m(\bar{s})\,e^{i\bar{s}\bar{x}}\,d\bar{s} = \frac{\mu}{a}u_y^{(j)}(a\bar{x}) \tag{37b}$$

in which the previously defined parameters have been nondimensionalized by the length a, i.e.

$$\omega_c = a\omega/V_c, \quad \omega_j = a\omega/V_j \quad \text{and} \quad \bar{n}_j(\bar{s}) = (\bar{s}^2-\omega_j^2)^{1/2}, \quad j = 1,2,3. \tag{38}$$

With a view toward reducing eqns (37) into algebraic equations, they are multiplied by the normalizing function $(1-\bar{x}^2)^{-1/2}T_l(\bar{x})$, where l is an integer, and an integration is performed over the interval $|\bar{x}| \leqslant 1$. After an interchange in the order of integration and using relation (36), the following set of independent algebraic equations is obtained:

$$\sum_n \mathscr{A}_{nl}A_n^{(j)} - \sum_m \mathscr{C}_{ml}B_m^{(j)} = \frac{2\mu}{a\pi}\int_{-1}^{1}\frac{u_x^{(j)}(a\theta)}{\sqrt{(1-\theta^2)}}T_l(\theta)\,d\theta \tag{39a}$$

$$\sum_n \mathscr{C}'_{nl}A_n^{(j)} + \sum_m \mathscr{B}_{ml}B_m^{(j)} = \frac{2\mu}{a\pi}\int_{-1}^{1}\frac{u_y^{(j)}(a\theta)}{\sqrt{(1-\theta^2)}}T_l(\theta)\,d\theta. \tag{39b}$$

In eqns (39), the coefficients $\mathscr{A}_{nl}, \ldots, \mathscr{B}_{nl}$ denote integrals defined over the interval $(-\infty, \infty)$. The integrands of these integrals are either odd or even and hence the range of integration can be reduced. It follows that $\mathscr{A}_{nl}$ and $\mathscr{B}_{nl}$ vanish for odd values of $(n+1)$, and for even values they are given by

$$\mathscr{A}_{nl} = (-1)^l \mathrm{i}^{n+l} \int_0^\infty \frac{4\gamma\omega_c^2 \bar{n}_3(\bar{s})}{F(\bar{s})} J_n(\bar{s}) J_l(\bar{s})\, \mathrm{d}\bar{s} \tag{40a}$$

$$\mathscr{B}_{nl} = (-1)^l \mathrm{i}^{n+l} \int_0^\infty \frac{2\omega_3^2[\beta_2 \bar{n}_1(\bar{s}) - \beta_1 \bar{n}_2(\bar{s})]}{F(\bar{s})} J_n(\bar{s}) J_l(\bar{s})\, \mathrm{d}\bar{s} \tag{40b}$$

similarly, $\mathscr{C}_{nl}$ and $\mathscr{C}'_{nl}$ vanish for even values of $(n+1)$ while for odd values of $(n+1)$, they are evaluated from

$$\mathscr{C}_{nl} = (-1)^l \mathrm{i}^{n+l+1} \int_0^\infty \frac{2\bar{s} F_1(\bar{s})}{F(\bar{s})} J_n(\bar{s}) J_l(\bar{s})\, \mathrm{d}\bar{s} \tag{41a}$$

$$\mathscr{C}'_{nl} = (-1)^l \mathrm{i}^{n+l+1} \int_0^\infty \frac{2\bar{s} F_2(\bar{s})}{F(\bar{s})} J_n(\bar{s}) J_l(\bar{s})\, \mathrm{d}\bar{s}. \tag{41b}$$

For a strip in smooth contact with the half-space, the coefficients $\mathscr{C}_{nl} = \mathscr{C}'_{nl} = 0$ and eqns (39) uncouple and immediately yield the coefficients $A_n^{(j)}$ and $B_n^{(j)}$.

The next step in the analysis is to confirm that integrals (40) and (41) are amenable to numerical treatment. For this purpose, expanding the integrands asymptotically for small and large values of $\bar{s}$, it can be readily shown that the integrands are well behaved at both limits of integration. In the absence of hysteretic damping of the medium, the roots of the Rayleigh function, $F(\bar{s})$, are in general complex (Jones, 1961). For the material parameters and hysteretic damping ratios used in this paper, the roots of $F(\bar{s})$ are all complex and lie outside the $\bar{s}$-axis. Hence, numerical evaluation of integrals (40) and (41) can be carried out in a routine manner. In order to assure rapid convergence at the upper limit of integration, the integrands are expanded for large values of $\bar{s}$ and the integrals containing the lowest order terms are evaluated in closed form using the result listed in Erdelyi *et al.* (1954). The remaining integrals are found to converge very rapidly and smoothly. Note that integrals (40) and (41) need be computed only once at each specified frequency.

The integrals appearing in the forcing terms of eqns (39) can be easily evaluated using the orthogonality relations of the Chebyshev polynomials

$$\int_{-1}^{1} (1-\bar{x}^2)^{-1/2} T_m(\bar{x}) T_n(\bar{x})\, \mathrm{d}\bar{x} = \begin{cases} \pi, & m = n = 0 \\ \pi/2, & m = n > 0 \\ 0, & m \neq n. \end{cases} \tag{42}$$

The orthogonality relations (42) can also be used to show that the influence functions are related to the expansion coefficients of the series representation of the contact stress distributions. In particular

$$\begin{aligned} H^{(j)} &= \pi a A_0^{(j)}/\mu \\ F^{(j)} &= \pi a B_0^{(j)}/\mu \\ M^{(j)} &= \pi B_1^{(j)}/2\mu. \end{aligned} \tag{43}$$

Here, the forces, $H^{(j)}$, $F^{(j)}$, are normalized by the shear modulus μ and the moment, $M^{(j)}$, is normalized by (μa^2). The real part of $H^{(j)}$ gives the stiffness corresponding to the horizontal mode of motion of the strip while the imaginary part, Im $H^{(j)}$, gives the corresponding damping coefficients of the medium. Similar interpretations can be given to the remaining influence functions.

This is as far as the solution can be analytically developed. Approximate (numerical) solutions for $A_n^{(j)}$ and $B_n^{(j)}$ in eqns (39) can be obtained by truncating the series expansions at the same number of terms and solving the resulting algebraic equations.

7. NUMERICAL RESULTS AND DISCUSSION

The remaining part of the paper is concerned with presenting numerical results for representative influence functions. Calculations were performed to compute the stiffnesses and radiation damping coefficients of the medium, which are the real and imaginary parts, respectively, of the influence functions, for dimensionless input frequencies in the range 0–5. The dimensionless frequency, $\bar{\omega}$, is defined as $\bar{\omega} = a\omega/V_s$, where $V_s = \mu/\rho$, the shear wave velocity in the bulk material. Three hysteretic damping ratios of the medium (λ_c) were considered, namely, 0, 5 and 10%. In order to explore the influence of permeability on the interaction coefficients, two cases of permeability (k) of 0.1 and 0.001 cm s^{-1} were examined. These two limiting values can be considered as representing permeability coefficients for typical sands. In all cases considered, the applied loads have been normalized by the shear modulus μ and the moment by (μa^2). In addition, the following material parameters, appropriate to saturated dense sand, have been assumed throughout the present work:

$$\nu = 0.25$$

$$\alpha = 1 \text{(saturated porous material)}$$

$$\alpha' = 293.9 \times 10^3 \text{ psi}$$

$$f = 0.35$$

$$\rho = 0.11937 \times 10^{-3} \text{ lb s}^2 \text{ in.}^{-4}$$

$$\rho' = 0.0327 \times 10^{-3} \text{ lb s}^2 \text{ in.}^{-4}$$

$$E_c = 14 \times 10^3 \text{ psi}$$

$$a = 300 \text{ in.}$$

In carrying out the numerical work, several terms of series expansions (35) were tried out and in each case the convergence was tested. It was concluded that by retaining four terms, adequate accuracy, within less than 1% is attainable in all cases. The numerical convergence of the integrals appearing in eqns (40) and (41) at the upper limit was improved by the scheme outlined previously. For a smooth contact between the strip and the half-space, extremely good convergence was observed in solving eqns (39), and somewhat slower convergence was encountered in the welded case. In the limiting case of a dry half-space ($\lambda_c \neq 0$), the following parameters are used to remove the influence of the pore fluid: $p = \rho' = \alpha' = \gamma' = a_j\,(j = 1, 2, 3) = 0$. One of the compression waves is eliminated (the one associated with n_2 in eqn (18)), and V_c, V_s reduce, respectively, to the usual longitudinal and shear velocities in an elastic medium. The behavior of the influence at $\bar{\omega} = 0$ are outlined in Appendix B. Essentially, it is found that the influence functions for horizontal and vertical modes of motion vanish at zero frequency while the stiffness function for the rocking mode remains finite.

Figures 2–4 display the influence functions for the horizontal, vertical and rocking modes of motion of a smooth strip. In these figures, the hysteretic damping ratio of the medium is assumed zero ($\lambda_c = 0$) and $k = 0.01$ cm s^{-1}. The top part of Fig. 2 represents the horizontal stiffness ($K_{HH} = \text{Re } H^{(5)}$), which is the horizontal force per unit length of the strip required to cause a unit horizontal displacement. The lower part of Fig. 2 represents the horizontal damping coefficient ($C_{HH} = \text{Im } H^{(5)}$). Figures 2–4 also contain the influence functions pertaining to a dry elastic medium over a frequency range of 0–3. These are shown dotted in the figures and were obtained from Oien (1970). The impact of pore fluid on the response of the medium is illustrated by comparing the dotted and solid curves. In Fig. 2, the effective stiffness of the two-phase medium is about 50–100% higher than the corresponding value of the dry medium while there is no appreciable change in the damping coefficients between the two cases. Figures 3 and 4 reveal a higher increase in the damping coefficient for the saturated medium, especially at the higher end of the frequency range. The increase is about 150%. Also, the stiffness changes sign at the higher frequencies for both the vertical and rocking modes of motion. Except for the damping coefficient in the

horizontal motion, these results are in qualitative agreement with those obtained by Lung (1980) and Costantino (1986). Note that the interaction coefficients presented by these authors need to be multiplied by π (see eqn (43)) for comparison with the results of Figs 2–4. Since in Figs 2–4 no hysteretic damping of the material was included, the variation in the interaction coefficients is entirely due to the presence of the pore fluid and its permeability effects.

In order to explore the effects of both hysteretic damping and complete and partial contacts between the strip and half-space, the interaction coefficients were computed for both models with $k = 0.01$ cm s^{-1} and $\lambda_c = 5\%$, and the results are shown in Figs 5–7. In this case, there is a change in sign of the stiffnesses for the horizontal and rocking modes of motion at about $\bar{\omega} = 2$ while in the vertical mode, the change in sign shifts towards the origin. This can be attributed to the influence of structural damping of the medium on the

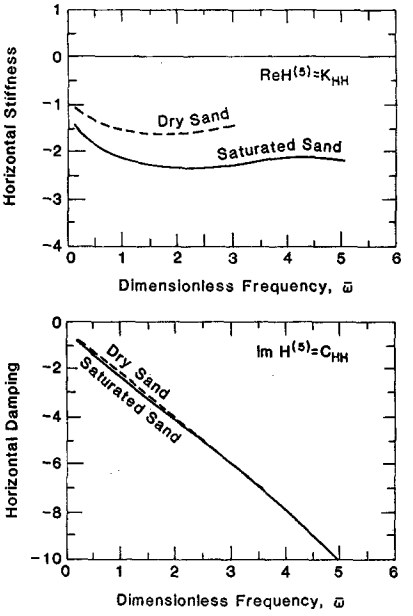

Fig. 2. Influence functions $H^{(5)}$ for smooth contact, $k = 0.01$ cm s^{-1} and $\lambda_c = 0\%$ (horizontal motion).

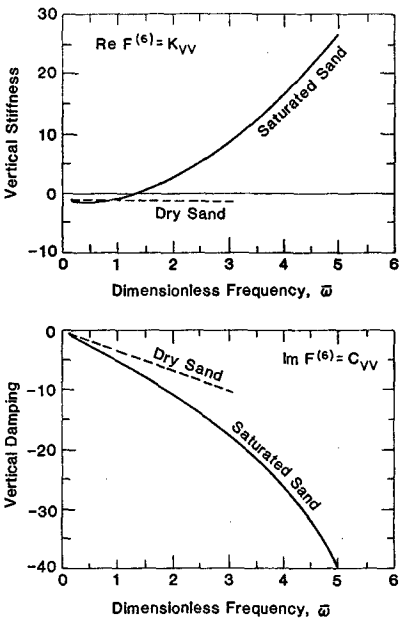

Fig. 3. Influence functions $F^{(6)}$ for smooth contact, $k = 0.01$ cm s^{-1} and $\lambda_c = 0\%$ (vertical motion).

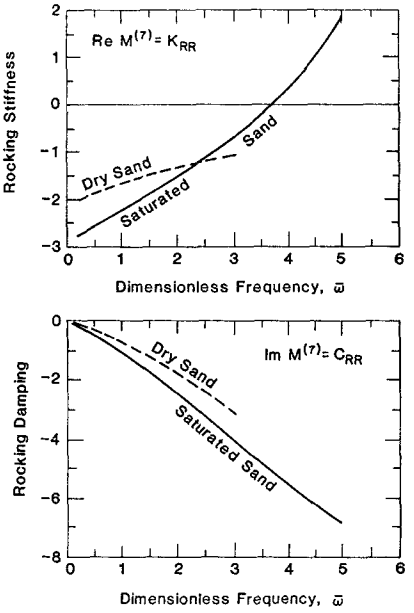

Fig. 4. Influence functions $M^{(7)}$ for smooth contact, $k = 0.01$ cm s^{-1} and $\lambda_c = 0\%$ (rocking motion).

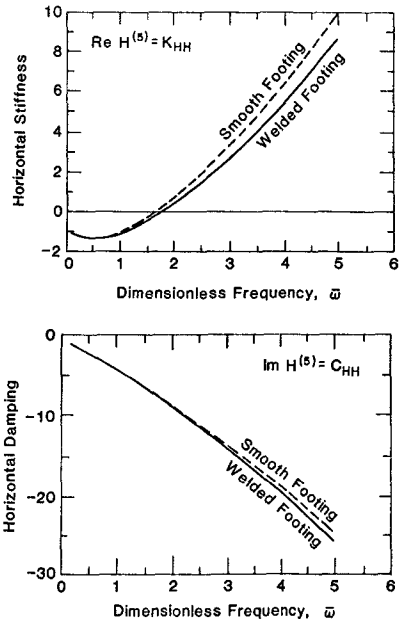

Fig. 5. Influence functions $H^{(5)}$ for welded and smooth contacts. Saturated sand, $k = 0.01$ cm s^{-1} and $\lambda_c = 5\%$ (horizontal motion).

response. Also, the magnitudes of the interaction coefficients for the three modes of motion show a monotonic increase with increasing values of $\bar{\omega}$. Concerning the impact of the types of contact, it is interesting to observe that the interaction coefficients in both models of contact are practically identical over the frequency range of interest in most seismic analysis problems (i.e. up to $\bar{\omega} = 3$ Hz). For a higher range of values of $\bar{\omega}$, there is appreciable deviation in the values of the stiffnesses only between the two contact models, especially in the vertical and rocking modes of the motion.

The variation of the influence function $H^{(7)}$ (which is equivalent to $M^{(5)}$) with the wave number $\bar{\omega}$ is shown in Fig. 8. This function reveals the coupling effect between the horizontal translational and rocking motions of a perfectly bonded strip to the medium. Based on the classical reciprocity theorem in elastodynamics, one would expect identical numerical values of the functions $H^{(7)}$ and $M^{(5)}$ in the present formulation. Indeed, the actual numerical

computation of both these coefficients gave reasonable accuracy. Figure 9 shows the effect of increasing the hysteretic damping ratio of the medium (λ_c) on the variation of the coupled stiffness and coupled damping coefficient with $\bar{\omega}$. In obtaining the results of Fig. 9, λ_c is assumed to be 10%. As expected, both interaction coefficients maintain the same shape. The coupled stiffness, however, is much larger than the previous case ($\lambda_c = 5\%$) while the damping coefficient, C_{HR}, is not significantly affected by increasing λ_c to 10%.

Figures 10–13 show the impact of including hysteretic damping of the dry medium ($k = 0$, $\lambda_c = 5\%$) on the interaction coefficients. The following conclusions can be made.

(1) The smooth and welded contact gave almost identical results.
(2) The character of the dry horizontal stiffness has changed.

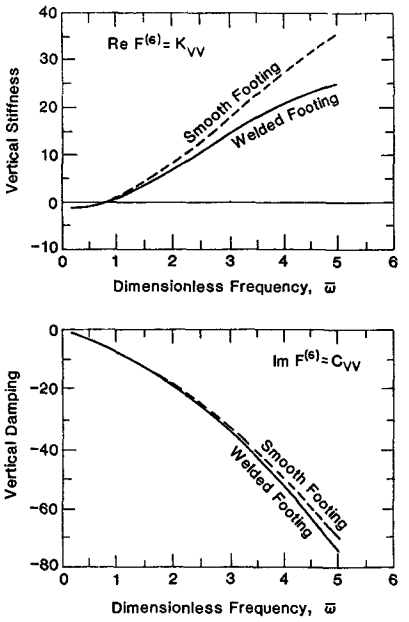

Fig. 6. Influence functions $F^{(6)}$ for welded and smooth contacts. Saturated sand, $k = 0.01$ cm s^{-1} and $\lambda_c = 5\%$ (vertical motion).

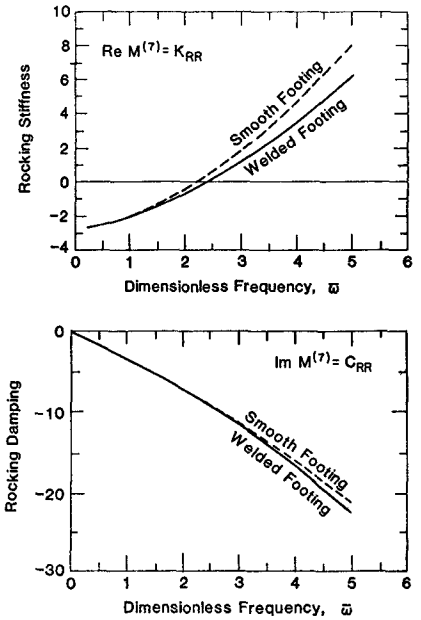

Fig. 7. Influence functions $M^{(7)}$ for welded and smooth contacts. Saturated sand, $k = 0.01$ cm s^{-1} and $\lambda_c = 5\%$ (rocking motion).

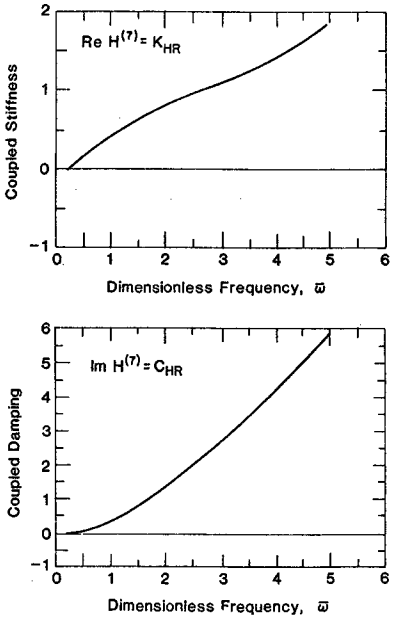

Fig. 8. Influence functions $H^{(7)} = M^{(5)}$ for welded contact. Saturated sand $k = 0.01$ cm s^{-1} and $\lambda_c = 5\%$.

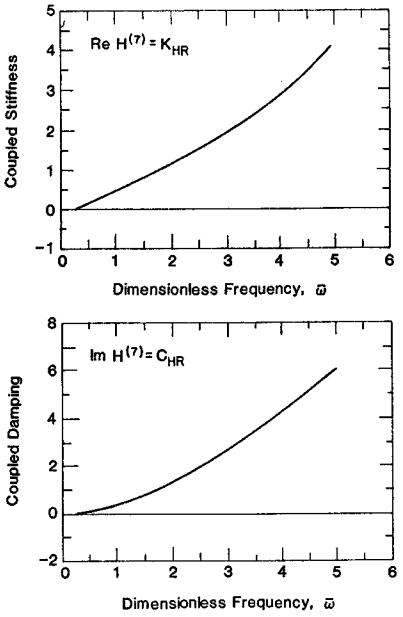

Fig. 9. Influence functions $H^{(7)} = M^{(5)}$ for welded contact. Saturated sand, $k = 0.01$ cm s^{-1} and $\lambda_c = 10\%$.

(3) A reduction of about 30–100% in the effective stiffnesses and damping coefficients is observed in the vertical and rocking modes of motion for both types of contact compared to the corresponding cases where $k = 0.01$ cm s^{-1}. The increase in the effective influence functions in the latter case is totally attributable to permeability effects and pore fluid stiffnesses. This clearly occurs near the higher values of the wave number $\bar{\omega}$ considered in this study. As can be concluded from Figs 5 and 10, the pore fluid has no major impact on the response due to horizontal motion of the strip.

The effects of varying the coefficient of permeability (k) on the interaction functions are exhibited in Figs 14–17 for the basic modes of motion of the strip. The computations were carried out for a welded strip atop a medium with $\lambda_c = 5\%$ and two values of k, namely, $k = 0.1$ and 0.001 cm s^{-1} were examined. These two values correspond to seepage

in soils consisting of typical medium and fine sands, respectively. The dotted curves correspond to $k = 0.1$ cm s^{-1}. It is clear from Figs 14–17 that only in the rocking motion there is an appreciable difference between the influence functions throughout the range of the frequency considered. As to be expected, the coupled stiffness, K_{RH}, and the coupled damping coefficients, C_{RH}, are strongly influenced by the speed of seepage of the pore fluid. Effects of varying the permeability (k) on smooth contact between the strip and the medium were also studied. However, the results are not significantly different from the welded case and are not reported here.

Finally, it should be pointed out that the solution presented here assumes that the footing is permeable. For an impermeable footing, an additional condition must be specified beneath the footing, namely, there be no flow out of the medium in that region. This

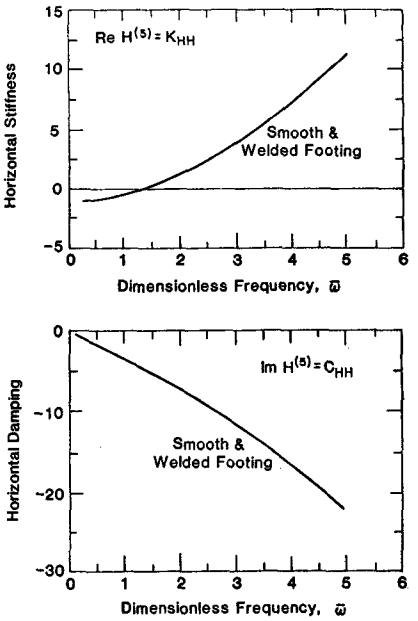

Fig. 10. Influence functions $H^{(5)}$ for welded and smooth contacts. Dry sand, $\lambda_c = 5\%$ (horizontal motion).

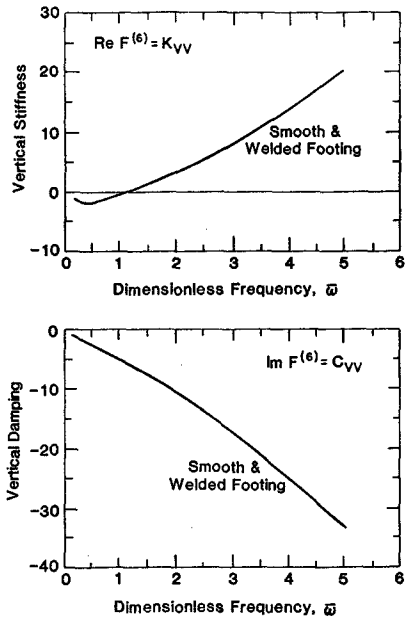

Fig. 11. Influence functions $F^{(6)}$ for welded and smooth contacts. Dry sand, $\lambda_c = 5\%$ (vertical motion).

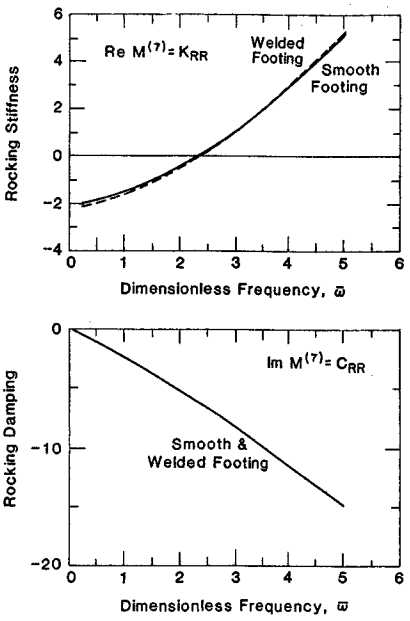

Fig. 12. Influence functions $M^{(7)}$ for welded and smooth contacts. Dry sand, $\lambda_c = 5\%$ (rocking motion).

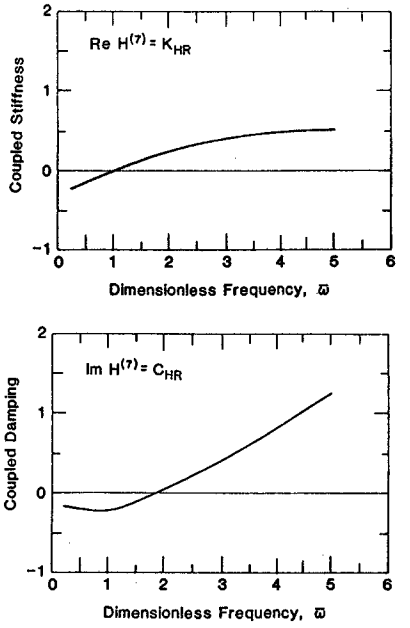

Fig. 13. Influence functions $H^{(7)} = M^{(5)}$ for welded contact. Dry sand, $\lambda_c = 5\%$.

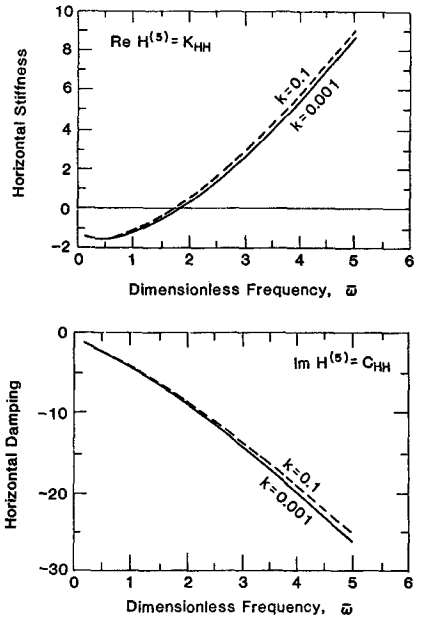

Fig. 14. Influence of permeability on interaction coefficients $H^{(5)}$ for welded contact (sand, $\lambda_c = 5\%$).

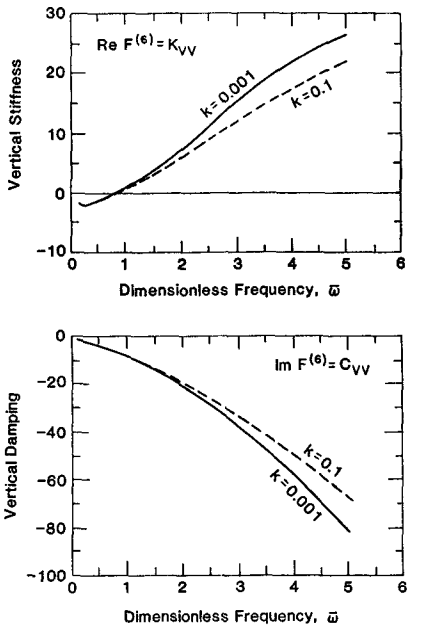

Fig. 15. Influence of permeability on interaction coefficients $F^{(6)}$ for welded contact (sand, $\lambda_c = 5\%$).

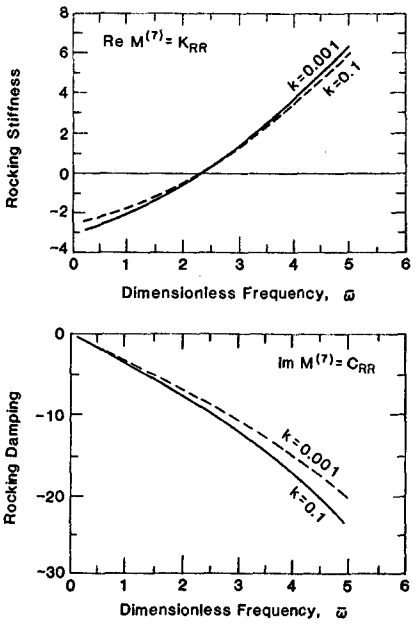

Fig. 16. Influence of permeability on interaction coefficient $M^{(7)}$ for welded contact (sand, $\lambda_c = 5\%$).

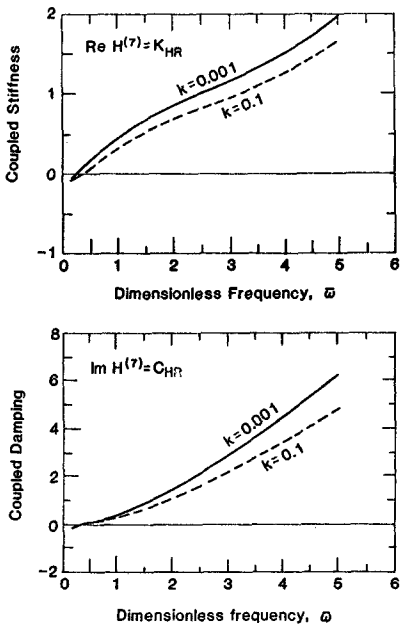

Fig. 17. Influence of permeability on coupling function $H^{(7)}$ for welded contact (sand, $\lambda_c = 5\%$).

condition would then lead to another integral equation beside the ones given here which would determine the pressure beneath the strip.

Acknowledgement—The authors would like to thank the referee for his constructive comments.

REFERENCES

Awjobi, A. O. and Grootenhuis, P. (1965). Vibrations of rigid bodies on semi-infinite elastic media. *Proc. R. Soc. Lond.* **287A,** 27–63.

Biot, M. A. (1956). Theory of propagation of elastic waves in a fluid-saturated porous solid: I—low frequency range. *J. Acoust. Soc. Am.* **28,** 168–178.

Biot, M. A. (1962). Mechanics of deformation and acoustic propagation in porous media. *J. Appl. Phys.* **33,** 1482–1498.

Collins, W. D. (1962). The forced torsional oscillations of an elastic half-space and an elastic stratum. *Proc. Lond. Math. Soc.* **12,** 226–244.

Costantino, C. J. (1986). Influence of ground water on soil–structure interaction. Report NUREG/CR-4588, BNL-NUREG-51983, Vol. 3.

Das Gupta, G. (1980). Foundation impedance matrices by substructure deletion. *J. Engng Mech. Div. ASCE* **106,** 517–526.

Deresiewicz, H. (1962). The effect of boundaries of wave propagation in a liquid–fluid porous solid: IV—surface waves in a half-space. *Bull. Seism. Soc. Am.* **52,** 627–638.

Erdelyi, A. *et al.* (1954). *Tables of Integral Transforms*, Vols 1 and 2. McGraw-Hill, New York.

Gladwell, G. M. L. (1968). Forced tangential and rotatory vibration of a rigid circular disk on a semi-infinite solid. *Int. J. Engng Sci.* **6,** 591–607.

Jones, J. P. (1961). Rayleigh waves in a porous, elastic, saturated solid. *J. Acoust. Soc. Am.* **33,** 959–962.

Junger, M. C. (1953). Concept of radiation scattering and its application to reinforced cylindrical shells. *J. Acoust. Soc. Am.* **25,** 899–896.

Karasudhi, P., Keer, L. M. and Lee, S. L. (1968). Vibratory motion of a body on an elastic half-space. *J. Appl. Mech. ASME* **35,** 697–705.

Lamb, H. (1904). On the propagation of tremors over the surface of an elastic solid. *Phil. Trans. R. Soc. Lond.* **203A,** 1–42.

Luco, J. E. and Westmann, R. A. (1972). Dynamic response of a rigid footing bonded to an elastic half-space. *J. Appl. Mech. ASME* **39,** 527–534.

Lung, R. H. (1980). Seismic analysis of structures embedded in saturated soils. Ph.D Dissertation, Department of Civil Engineering, City University of New York.

Muskhelishvili, N. I. (1953). *Some Basic Problems of the Mathematical Theory of Elasticity*. Noordhoff, Groningen, The Netherlands.

Oien, M. A. (1970). Steady motion of a rigid strip bonded to an elastic half-space. *J. Appl. Mech. ASME* **38,** 328–334.

Paul, S. (1976a). On the displacements produced in a porous elastic half-space by an impulsive line load (non-dissipative case). *Pure Appl. Geophys.* **114,** 605–614.

Paul, S. (1976b). On the disturbance produced in a semi-infinite poroelastic medium by a surface load. *Pure Appl. Geophys.* **114,** 615–627.

Robertson, I. A. (1966). Forced vertical vibration of a rigid circular disk on a semi-infinite elastic solid. *Proc. Camb. Phil. Soc.* **62A,** 547–553.

Smith, P. W., Jr. (1962). Response and radiation of structural modes excited by sound. *J. Acoust. Soc. Am.* **34,** 640–645.

Thau, S. A. (1967). Radiation and scattering from a rigid inclusion in an elastic medium. *J. Appl. Mech. ASME* **34,** 509–511.

Williams, M. L. (1959). The stresses around a fault or crack in dissimilar media. *Bull. Seism. Soc. Am.* **49,** 199–204.

Zakorko, V. N. and Rostovtsev, N. A. (1965). Dynamic contact problem of steady vibrations of an elastic half space. *J. Appl. Math. Mech.* **29,** 644–653.

APPENDIX A: ALGEBRAIC ABBREVIATIONS

The abbreviations introduced in this paper (for algebraic convenience) are described here.

(1) Values of V_j and a_j: the complex-valued velocities, V_j ($j = 1, 2, 3$), appearing in eqns (15) and (17) stand for

$$V_j = V_c/\lambda_j, \quad j = 1, 2, 3 \tag{A1}$$

where the "confined velocity" V_c stands for

$$V_c = (E_c + \alpha^2\alpha')/\rho \tag{A2}$$

and

$$\lambda_{1,2} = [B-(1+i\omega KE_c\lambda_c/\alpha')i\gamma'/(k\rho\omega) \mp \Delta]/(2A) \tag{A3}$$

$$\lambda_3 = [C-i\gamma'/(k\rho\omega)]/\{c_2KE_c(1+i\omega\lambda_c)[N/f-i\gamma'/(k\rho\omega)]/\alpha'\}. \tag{A4}$$

In eqns (A3) and (A4), the following contractions are made:

$$A = K(1-\alpha^2K+i\omega KE_c\lambda_c/\alpha') \tag{A5}$$

$$B = K+N(1+i\omega KE_c\lambda_c/\alpha')/f-2\alpha KN \tag{A6}$$

$$C = N/f-N^2 \tag{A7}$$

$$\Delta^2 = B^2-4AC-2i[-2A+B(1+i\omega KE_c\lambda_c/\alpha')]\gamma'(k\rho\omega)-(1+i\omega KE_c\lambda_c/\alpha')^2(\gamma'/k\rho\omega)^2. \tag{A8}$$

Similarly, the coefficients a_j ($j = 1, 2, 3$) appearing in eqns (14) and (16) designate the quantities

$$a_j = [1-\alpha N-\lambda_j(1-\alpha^2K+i\omega KE_c\lambda_c/\alpha')]/[\alpha N/f-N-i\alpha\gamma'/(k\rho\omega)], \quad j = 1,2 \tag{A9}$$

$$a_3 = N[i\gamma'/(k\rho\omega)-N/f]^{-1}. \tag{A10}$$

(2) Expressions for $\beta_j(s,\omega), j = 1, 2$ and $\gamma(s,\omega)$ in eqns (21) and (22) are

$$\beta_j = \lambda_j(a_j+\alpha)/[\lambda_2(a_2+\alpha)-\lambda_1(a_1+\alpha)], \quad j = 1,2 \tag{A11}$$

$$\gamma = \{\lambda_1\beta_2[\alpha\alpha'(a_1+\alpha)-E_c(1+i\omega\lambda_c)]-\lambda_2\beta_1[\alpha\alpha'(a_2+\alpha)-E_c(1+i\omega\lambda_c)]\}/[2c_2E_c(1+i\omega\lambda_c)]. \tag{A12}$$

APPENDIX B: BEHAVIOR OF INFLUENCE FUNCTIONS FOR $\bar{\omega} = 0$

In order to determine the values of the influence functions as $\bar{\omega} \to 0$, examine the limiting behavior of the coefficients $\mathscr{A}_{nl}$, $\mathscr{B}_{nl}$, etc. in eqns (39). For the coefficient, $\mathscr{A}_{nl}$, the asymptotic expression of eqn (40a) is

$$[\mathscr{A}_{nl}]_{\bar{\omega}\to 0} \sim \int_0^\infty \frac{1}{\bar{s}} J_n(\bar{s})J_l(\bar{s})\,d\bar{s}, \; n \text{ and } l = \text{integers}. \tag{B1}$$

Utilizing the values of integral (B1) listed in Erdelyi *et al.* (1954), it is readily confirmed that

$$[\mathscr{A}_{nl}]_{\bar{\omega}\to 0} \sim \begin{cases} \infty, & n = l = 0 \\ \text{finite}, & n \text{ or } l \neq 0. \end{cases} \tag{B2}$$

Similarly limiting values can be established for the coefficients $\mathscr{B}_{nl}$, etc. Hence, it can be concluded that the coefficients A_{00} and B_{00} approach infinity as $\bar{\omega} \to 0$, implying that coefficients A_0 and B_0 approach zero for the same frequency. It follows from eqns (43) that $H^{(j)}$ and $F^{(j)}$ vanish at $\bar{\omega} = 0$. Hence, the influence functions for the horizontal and vertical modes are zero at $\bar{\omega} = 0$. In a similar manner, it can be concluded that B_{11} is finite at the zero frequency and thus one can conclude the same for the rocking mode influence functions.